Proceedings of the
Annual Stability Conference
Structural Stability Research Council
Orlando, Florida, April 12-14, 2016

Experimental Studies on the Composite Action in Wood-Sheathed and Screw-Fastened Built-Up Cold-Formed Steel Columns

David C. Fratamico[1], Shahabeddin Torabian[2], Kim J. R. Rasmussen[3], Benjamin W. Schafer[4]

Abstract

This paper addresses an ongoing computational and experimental effort on the quantification of composite action in built-up cold-formed steel (CFS) columns used frequently in CFS framing. The section studied herein is a common back-to-back lipped channel section with two self-drilling screw fasteners connecting the webs of the individual studs. Previous elastic buckling studies concluded that for industry-standard built-up columns designed according to AISI S100-12 Section D1.2, up to 85% of fully composite action is achieved in global buckling. In recent testing detailed herein, the components of (and attached to) a built-up column as installed in a CFS frame such as tracks and sheathing were studied as they contribute to the increase in composite action and consequently, axial capacity of the columns. Sixteen monotonic, concentric compression tests of 2 standard sections at 6 ft [1.83 m] in length and with varying fastener layouts and sheathing conditions were performed. Column deformation was monitored using 17 strategically placed position transducers. Results indicate a large increase in composite action with the addition of OSB sheathing. In addition, built-up column-to-track connections as well as prescriptive end-fastener groupings designated by the specification provide a column end condition which more closely approximates a fixed end condition rather than the more commonly and conservatively assumed pin end condition. Future work includes two successive phases of testing which will compare a wide range of built-up section types to current design provisions and elucidate the effect of fastener spacing and layout on local and distortional buckling modes, as well as numerical modeling of fastener layouts in a finite strip modeling domain for use in design.

1. Introduction

Cold-formed steel (CFS) structural systems are mostly composed of thin-walled open sections that have high axial capacities while also being lightweight. Built-up sections are often assembled and used in low to mid-rise CFS buildings where heavy vertical loads or greater local system rigidity is required. They can also be designed as truss members, stand-alone columns, and chord studs in CFS-framed shear or exterior walls, and headers/jambs. Common built-up

[1] Graduate Research Assistant, Dept. of Civil Engineering, Johns Hopkins University, <fratamico@jhu.edu>
[2] Assistant Research Professor, Dept. of Civil Engineering, Johns Hopkins University, <torabian@jhu.edu>
School of Civil Engineering, College of Engineering, University of Tehran, <torabian@ut.ac.ir>
[3] Professor, School of Civil Engineering, University of Sydney, <kim.rasmussen@sydney.edu.au>
[3] Professor, Dept. of Civil Engineering, Johns Hopkins University, <schafer@jhu.edu>

members include the screw-fastened back-to-back "I" and toe-to-toe "box" sections, which are doubly symmetric, constructed using traditional lipped channel sections, and can offer an axial compression capacity of more than twice that of the individual members if composite action is enabled by the use of stud interconnectors: screws, bolts, welds, or battens. Although research on cold-formed steel built-up member behavior and design is increasingly appearing in the literature, a much greater body of existing work has studied the compound buckling behavior and slenderness ratio of hot-rolled steel built-up beams and columns. For example, Liu et al. (2009) validated experimentally that the slenderness ratio of an individual element in a built-up column must not exceed three-fourths of the overall member slenderness ratio, as per AISC-360 (2010).

Within the past decade, however, there has been a push towards studying the behavior of cold-formed steel columns since design rules for these types of members are limited in the current North American cold-formed steel specification (AISI-S100 2012). A limited set of column experiments with back-to-back CFS channel sections found that the AISI-S100 (2012) modified slenderness ratio can be conservative and that the end connections are critical for maintaining overall column strength (Stone and LaBoube 2005). Young and Chen (2008) conducted experiments on built-up CFS sections with intermediate stiffeners and concluded that using the Direct Strength Method (DSM) for calculating nominal local and distortional capacities using single section properties provided reliable and conservative estimates; composite action was not significant in their tests.

Other experimental tests, conducted in parallel with numerical analysis, on various types of built-up CFS column cross-sections using Z section studs have been completed and compression capacities compared with DSM-based equations that were calibrated to account for buckling interactions (Georgieva et al. 2012). Similar testing of varying cross-sections and DSM calibration was completed by Zhang (2014) at the University of Hong Kong, and efficient attempts to model web interconnections are explored. Also form the same research group in Hong Kong, the behavior and strength of built-up beams with back-to-back and box-section types made with varying screw arrangements, web perforations, and intermediate stiffeners were studied; parallel numerical models were completed and DSM design approaches were proposed. Global-local buckling interactions were closely observed and studied in Loughlan and Yidris (2014). Anbarasu et al. (2015) conducted similar experimental and numerical analyses on battened built-up CFS columns and assessed the conservatism of two DSM approaches, while also closely studying local and global deformations. Dabao et al. (2015) also conducted experiments and numerical analyses on pin-ended, back-to-back battened columns, concluding that AISI provisions are non-conservative for specimens failing in local buckling and conservative for those failing in flexural buckling. Reyes and Guzmán (2011) tested 48 weld-connected "box" sections and showed that the modified slenderness ratio of AISI S100 (2012) is not necessary when the base metal thickness is less than 2 mm and if the seam weld spacing is greater than 600 mm for box sections with any type of end condition tested. Li et al. (2014) completed experimental and numerical analyses of 2 types of built-up CFS sections made with both lipped and web-stiffened channel sections; one type had a back-to-back web configuration while the other was a screw-connected "box" section. They extended existing AISI-S100 (2012) design provisions for flexural and distortional buckling, and offered suggestions for optimal built-up member fastener spacing.

Sheathed built-up columns have not been extensively studied, but work on the axial compressive capacity of sheathed single studs (Vieira 2013) has been completed with emphasis on sheathing-braced design and quantification of both local and diaphragm stiffnesses for foundation springs used in elastic buckling analyses. Ye et al. (2016) conducted 16 full-scale single and "I" section built-up column tests with oriented strand board (OSB) sheathing and observed a prevalence of local and flexural-torsional buckling deformations, which are not accounted for in current design codes; these results are mostly confirmed by the experimental results reported herein.

While the 2005 AS/NZS standards have only a maximum fastener spacing requirement for CFS built-up column design, AISI-S100 (2012) Section D1.2 requires the calculation of the axial capacity of these columns using the modified slenderness ratio approach, as adopted from AISC 360 (2010) which assumes only flexural deformations.

$$\left(\frac{KL}{r}\right)_m = \sqrt{\left(\frac{KL}{r}\right)_o^2 + \left(\frac{a}{r_i}\right)^2} \tag{1}$$

In Eq. 1, $(KL/r)_o$ is the slenderness ratio of the entire composite section about its minor axis, a is the intermediate fastener spacing along the column height, and r_i is the minimum radius of gyration of each single stud within the built-up column. This modified slenderness is used to estimate the critical axial compressive load of built-up columns in minor-axis flexural buckling only; it assumes a loss of shear rigidity at the discrete fasteners and a penalty (increase) is applied to the slenderness ratio. It cannot predict the effects of fastener spacing/layouts on torsional, flexural-torsional, distortional, or local buckling modes. Built-up members in pure flexure are prescribed a maximum fastener spacing of the lesser of either $L/6$ or a factor dependent on the tensile strength of a single connection.

Although AISI-S100-12 obliges the use of a special fastener grouping at the member ends, the requirement is prescriptive and its impact on the modified slenderness is not treated directly. Section D1.2 specifies that screws in these end fastener groups must be longitudinally spaced no more than 4 diameters apart and for a distance equal to 1.5 times the maximum width of the member. AISI-S100-12 also imposes a maximum fastener spacing, a, along the length via Eq. 2. If the modified slenderness ratio (a higher value) is instead used in the following equation, an iterative calculation must be performed to arrive at an optimal fastener spacing. The Specification does not indicate if any of the fasteners are single or doubled within each fastener longitudinal spacing increment, but the doubled configuration is assumed in the work presented in this paper.

$$\frac{a}{r_i} \leq \frac{1}{2}\left(\frac{KL}{r}\right)_o \tag{2}$$

The work presented herein follows introductory numerical studies by the first author in which the level of compositeness was varied using both fixed constraints and discrete elastic springs as fasteners in Finite Element and Finite Strip-based models used for elastic buckling analyses (Fratamico and Schafer 2014). The partially composite realm was studied empirically in the past by Maia et al. (2012) and more extensively in a numerical study by Fratamico et al. (2015) where discrete fastener axial, shear, and rotational stiffnesses were modeled by means of a special

"fastener element" in a finite element analysis (elastic buckling and 2nd order elastic analysis) to quantify the level of composite action and estimate fastener demands in a column undergoing flexural buckling. A series of experimental studies are presented in this paper with the goal of understanding which components of a column, as constructed and installed in a traditional CFS structure, affect the composite action under concentrically-applied compressive loads. The two back-to-back channel sections used (362S162-68 and 600S137-54 using AISI-S200-12 nomenclature, note 362S162-68 has a 3.62 in. web, 1.62 in. flange, and material thickness of 0.068 in. nominal) are studied as single studs and also doubled studs with varying web interconnection layouts (using screws), with all columns built with or without OSB sheathing.

2. Built-Up Cold-Formed Steel Column Testing

In this paper, sixteen column tests are described and reported. These tests are part of a series of 3 phases of built-up CFS column testing at Johns Hopkins University through which studies on composite action, fastener spacing/layout, and column end conditions, as well as an extensive comparison to code-based predictions for strength are being performed. In this work (Phase 1), the progression of non-composite to partially or fully composite buckling behavior is studied. The test series requires monotonic, concentric compression loading using a 100 kip [445 kN] MTS universal testing rig. The column specimens are installed within tracks, which rest on fixed platen supports. Prevailing deformation modes are sought, as they develop under a certain fastener layout, end conditions, and presence of sheathing. The recommended fastener spacing and layout per AISI S100-12 is used for all trials, and the column length is fixed at 6 ft [1.83 m], the maximum length allowed in the MTS rig setup, in this test series.

2.1 Test Matrix and Instrumentation

Section types were selected to differ in local slenderness, but still be globally slender. The 362S162-68 is a popular cross-section in CFS buildings, but is not as locally slender when compared to the other selected cross-section, the 600S137-54. Both sections have also been tested in the senior author's structural lab in the past (Vieira (2013), Torabian et al. (2015)). Fig. 1 shows the typical arrangement of the built-up "I" sections and typical screw arrangements.

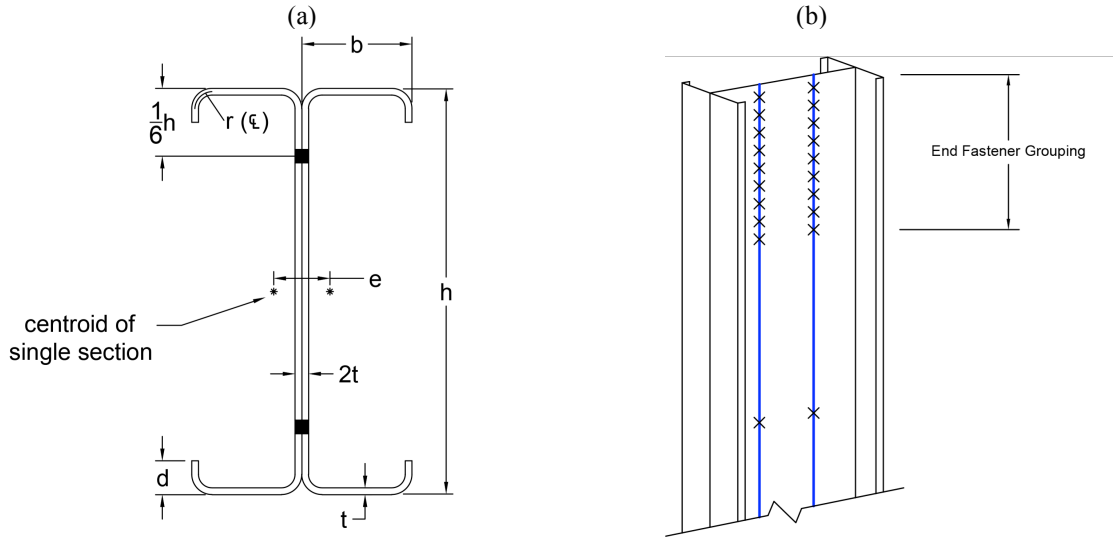

Figure 1: (a) The built-up, back-to-back section studied, showing the location of the web interconnections via screws and (b) an example of the AISI-recommended fastener layout at the column ends

Table 1: Test matrix

ID	Trial	Section		OSB	Single	Back-to-Back Interconnection		
		362S162-68	600S137-54			None	Even[a]	AISI[b]
1	A1	X			X			
2	A2	X				X		
3	A3	X					X	
4	A4	X						X
5	A5	X		X	X			
6	A6	X		X		X		
7	A7	X		X			X	
8	A8	X		X				X
9	B1		X		X			
10	B2		X			X		
11	B3		X				X	
12	B4		X					X
13	B5		X	X	X			
14	B6		X	X		X		
15	B7		X	X			X	
16	B8		X	X				X

[a]Evenly-spaced screw spacing
[b]Prescriptive AISI-based screw spacing

The test matrix is shown in Table 1, where at least 8 unique test cases are performed on the two types of sections used (see Fig. 2 for illustrations of the cases). The goal is to understand the effect of the incremental addition of assembly components that can contribute to composite action. The true stud-to-track semi-rigid end condition is tested via single stud tests A1 and B1. The back-to-back stud end condition with the track when no fasteners are present in the webs is tested via A2 and B2. The effect of intermediate fasteners whose spacing is designed according to AISI S100-12 D1.2 and E4.2 (see Fig. 2, case 3) is studied via trials A3 and B3. Lastly, the effect of end fastener groups on the developed composite action is studied in trials A4 and B4, with details on screw layouts in Fig. 2 (see case 4). The length of the end fastener groups from the ends of the member, per AISI, were calculated as: α = 5.44 in. [138 mm] and 9.00 in. [229 mm] for the 362S162-68 and 600S137-54 section trials, respectively; α is the maximum width of the column multiplied by 1.5. All trials are then repeated (as A5-A8 and B5-B8) with OSB sheathing of 7/16 in. [11.1 mm] thickness, attached on both sides of the studs and in contact with the stud flanges and track lips. Isolation plates (½ in. [12.7 mm] thick) were installed between the tracks and their adjacent platens, at the top and bottom of the column, to prevent bearing on the OSB ends. The purpose of the sheathed tests is to understand and quantify the achievable, upper bound composite action with the added effect of bracing and confinement of the sheathing on the built-up studs; local deformation modes are sought as well.

As per industry standard, studs are connected with steel-to-steel hex washer head screws (self-drilling #10) and between studs and tracks as well. For the specimens with OSB, the hex washer head screw is replaced with a steel-to-steel flat pancake head screw (Simpson FPHSD #10) so as to not bow the OSB as it is fastened over the track. OSB sheathing is attached with Simpson #10 PPSD wood-to-steel screws.

All tests are displacement-controlled with quasi-static loading. The load rate does not exceed 0.06 in/min [1.52 mm/min] for single studs or 0.03 in/min [0.76 mm/min] for back-to-back studs. Loading platens are made of low-carbon steel with an appropriate hardness and yield strength as required for the tests; they were made sure to be installed parallel (+/- 0.05° off the horizontal plane). The dimensions and setup are shown in Figures 3-5. Measurements of load are made through the load cell on the MTS rig (Fig. 3), and the MTS's LVDT measures the applied displacements. To track specimen deformations, 17 position transducers (PTs) are installed. Lateral bi-planar displacements and overall rotation at the mid-section can be tracked throughout the test using 11 PTs at mid-height (see Fig. 5). In addition, 1 PT is installed on the top and bottom tracks, orthogonal to the web of the studs in order to track the out-of-plane deformation of the webs due to local buckling or localized failures at the ends. To monitor stud engagement to the track during the tests, 2 PTs are installed: one at the top and one on the bottom track. Lastly, for unsheathed specimens, if flexural buckling is expected, a special "shear slip" PT is installed at the top and bottom to monitor the web slip for trials with different levels of composite action (see Figures 6 and 7 for the slip mechanism and setup). LabVIEW software and National Instruments hardware are used to coordinate all data acquisition. The error of eccentricity of the applied loads and out-of-plumbness are recorded for each column as they are loaded into the rig. Specifically, measurements were taken near the top, bottom, and mid-height of the columns in two planar directions to endure that the centroid of each column's section were within the line of action of the applied load in the rig. Upon final positioning, error values are recorded, but considered negligible since eccentricities were calculated as never larger than 0.025 in. [0.64 mm].

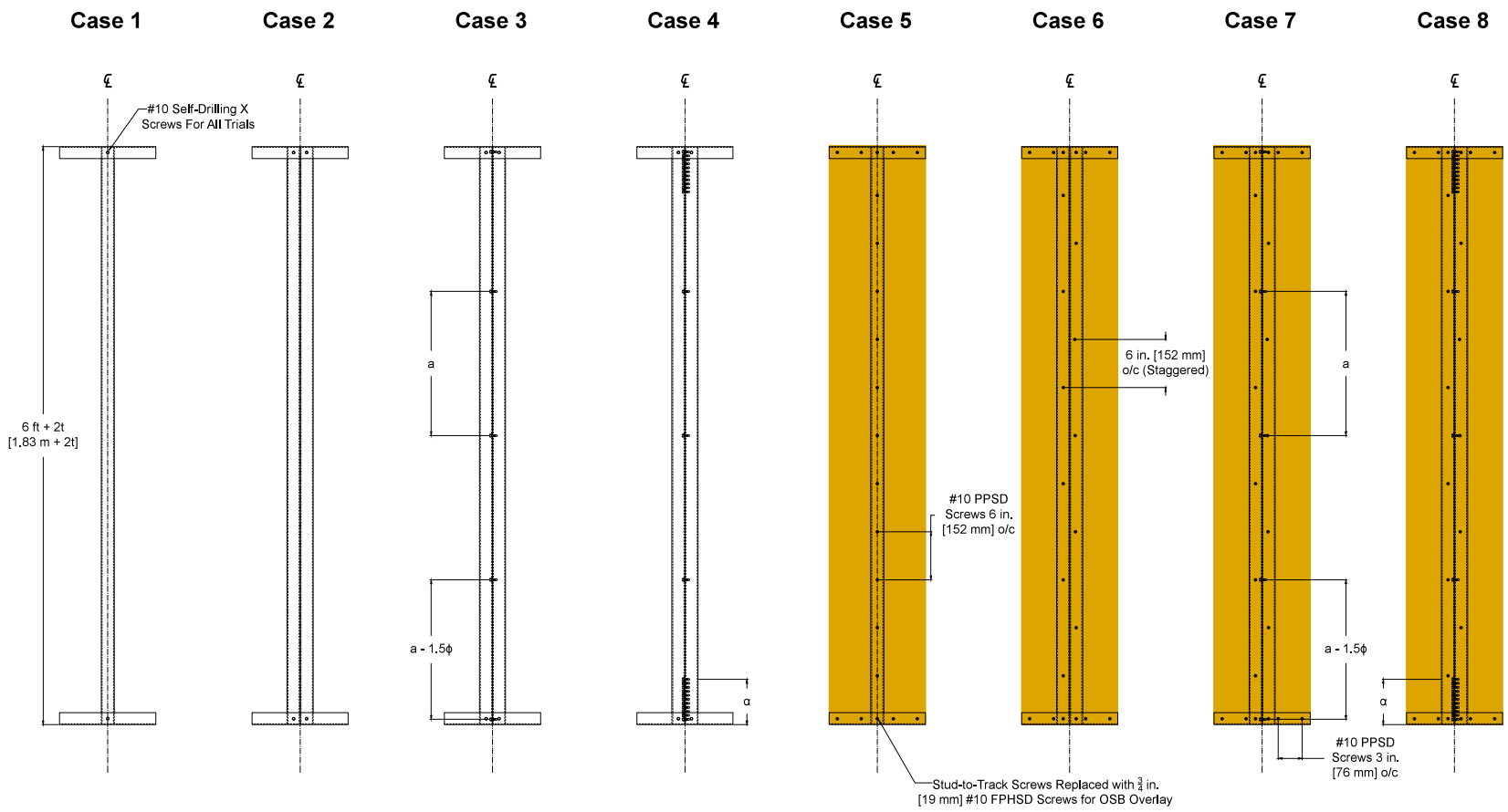

Figure 2: Cases 1-8 for each built-up column section tested, where: cases 5-8 are testing conditions 1-4 with OSB added, *a* is the fastener spacing, ϕ is the screw diameter, and α is the length of the end fastener group

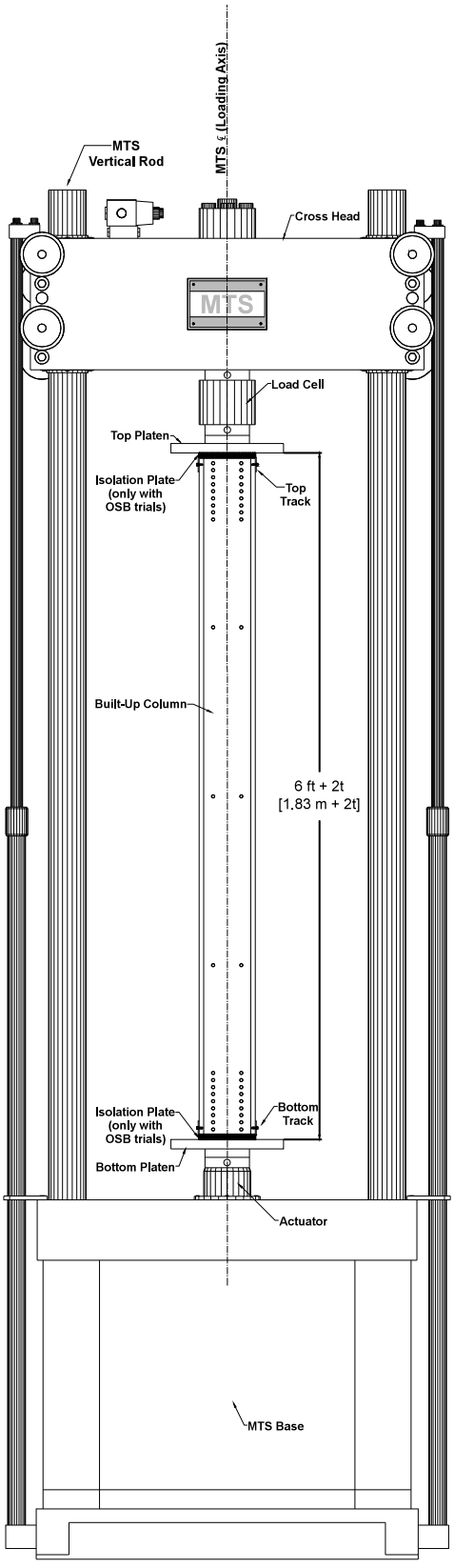

Figure 3: MTS test rig setup (elevation)

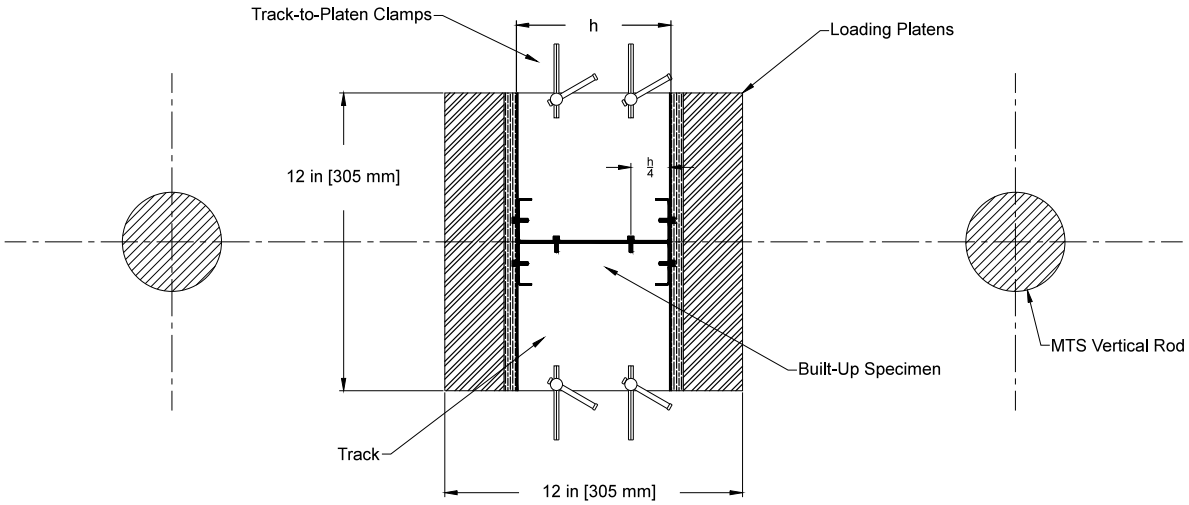

Figure 4: MTS test rig setup (top-down view)

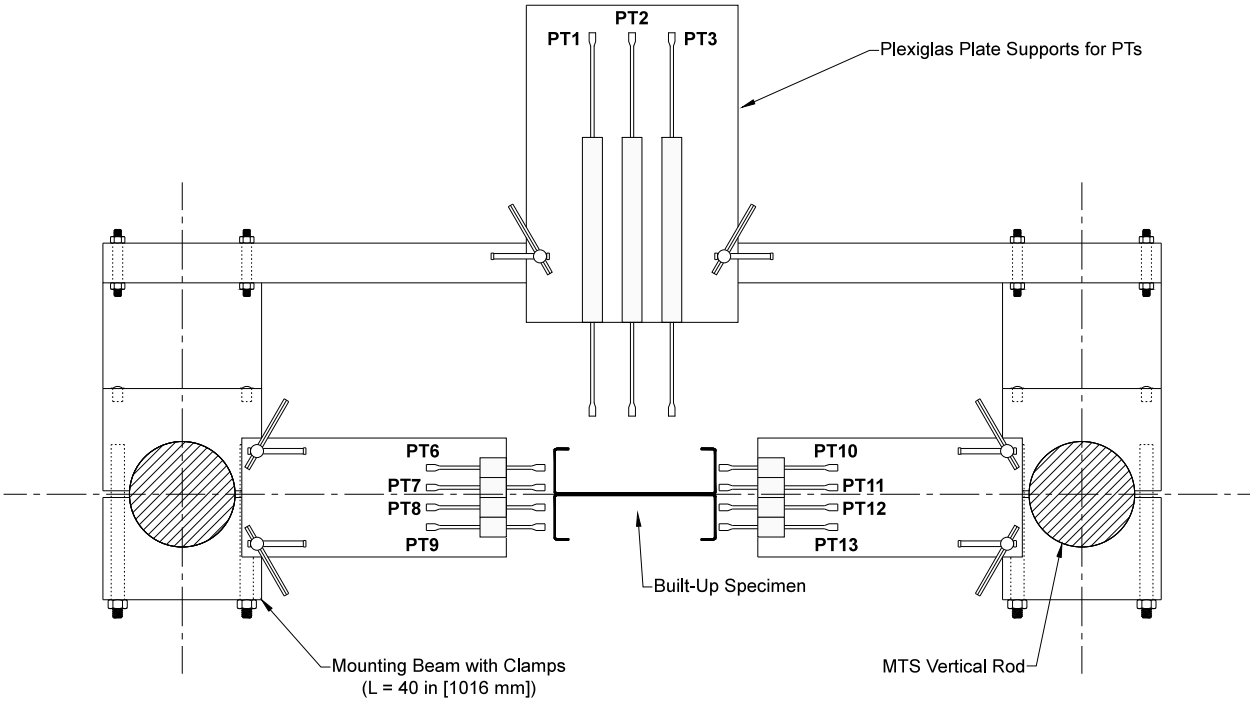

Figure 5: Position transducer setup at unsheathed column mid-height (top-down view)

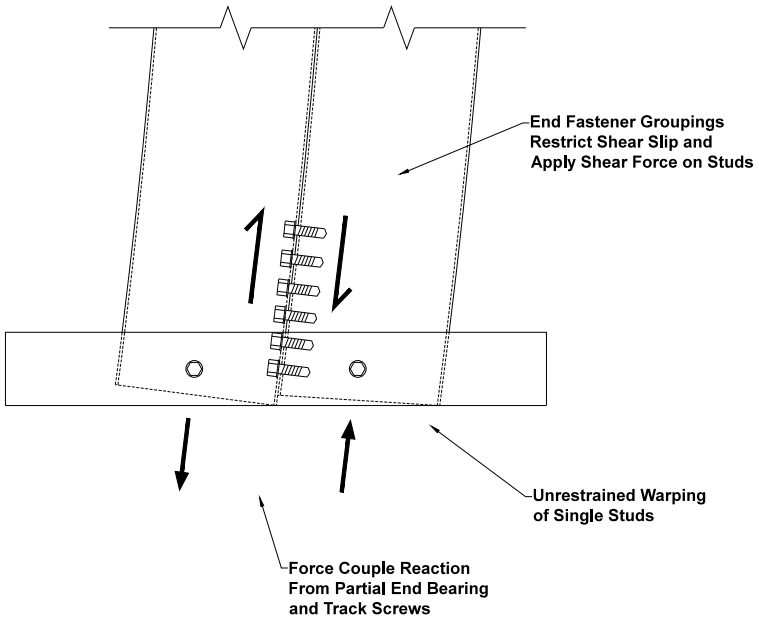

Figure 6: Shear slip expected when columns undergo flexural buckling

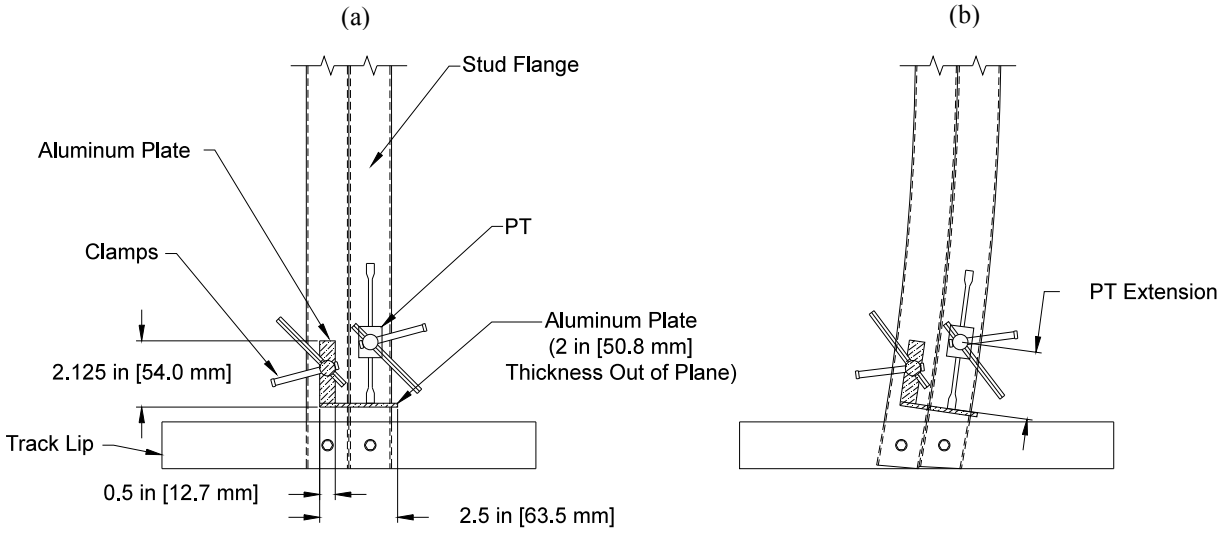

Figure 7: Setup for the "shear slip" position transducers in (a) an undeformed and (b) a deformed state

2.2 Laser Scanning for Geometric Imperfections

Measurements for specimen dimensions and quantification of geometric imperfections were completed using a novel laser scanning method. The laser scanner, shown in Fig. 8, uses a 2D line laser that generates 800 points per reading (longitudinal to the column) and a rotary stage allows for angled readings (Zhao 2015). Full-field 3D geometric information is obtained as a point cloud of stitched longitudinal scan readings from different scan angles. Example output data for cross-section dimensions are shown in Fig. 9. Average plate thickness for each specimen was measured by hand using a calibrated micrometer, and the results can be used in finite strip analyses and in the reconstruction of the 3D geometry for each specimen. Final results are not reported here since the scan data is currently being post-processed.

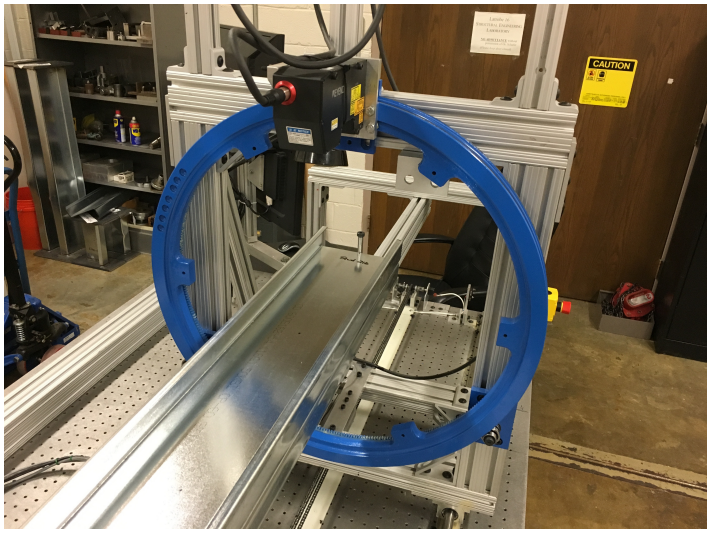

Figure 8: Laser scanner setup with built-up specimen installed

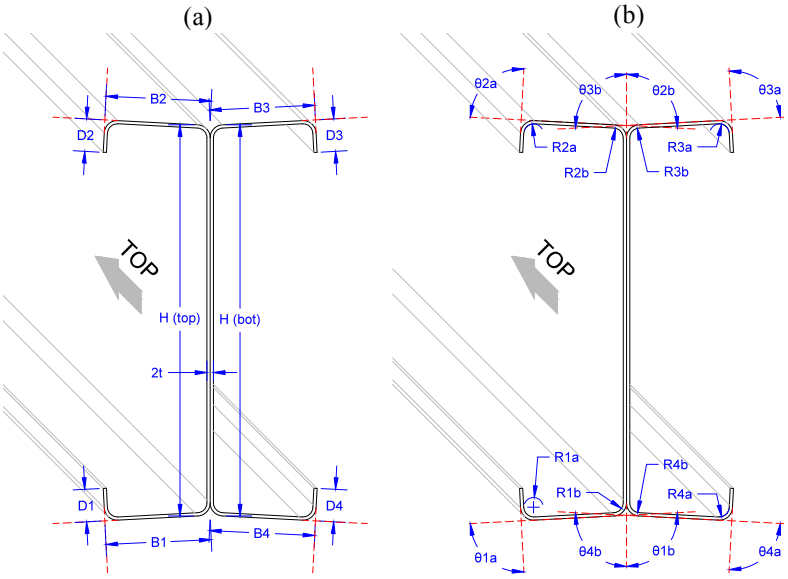

Figure 9: Planar cross-section dimensions averaged over longitudinal length: (a) lengths and (b) angles and radii

2.3 Coupon Testing for Material Characterization

To quantify basic material properties of the cold-formed steel used for the test specimens, a series of 16 coupon tests, using CNC milled longitudinal cuts of the webs and flanges for the channel sections and of the webs and lips of the track section, were performed. Fig. 10 shows the locations of the coupons. Testing was completed in accordance with ASTM A370-12a (2012), and results are shown in Table 2. To remove the zinc coating, both ends of all coupons were put in a 1M HCl solution until the coating was removed; uncoated steel measurements (namely uncoated thickness) could then be made. Fig. 11 shows the ASTM-dictated coupon dimensions for steel sheet thicknesses used in the tests herein. Yield (at 0.2% offset) and ultimate tensile strengths for the 362S162-68 and 362T125-68 sections were similar and recorded with a mean of 60.8 ksi [419.3 MPa] and 78.8 ksi [543.0 MPa], respectively. Similarly, for the 600S137-54 and 600T150-54 sections, yield and ultimate tensile strengths were recorded with a mean of 57.7 ksi [397.8 MPa] and 70.1ksi [483.0 MPa], respectively. All yield stress values are considerably above the nominal 50 ksi [344.7 MPa]. Young's modulus was not estimated from the linear data in the test results and is assumed to be 29,500 ksi [203.4 GPa] as prescribed in AISI S100-12.

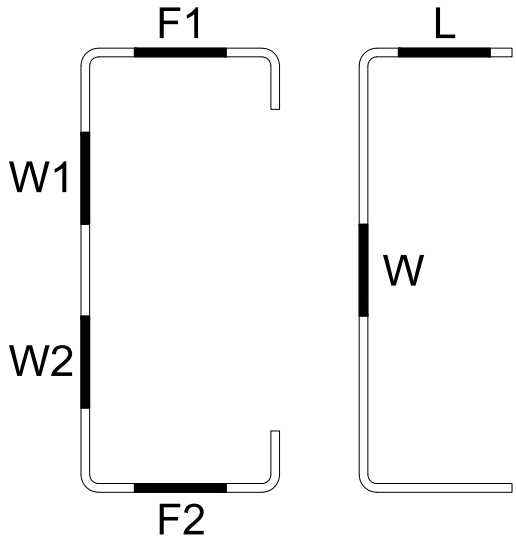

Figure 10: Location of coupon taken from the lipped channel (left) and track sections (right)

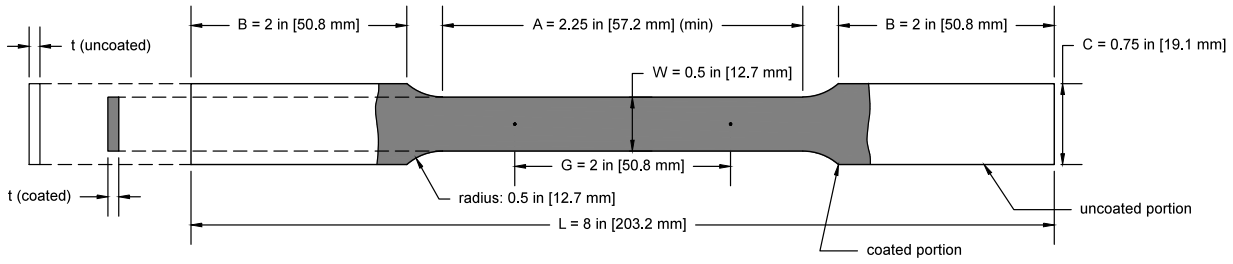

Figure 11: Tensile coupon dimensions

Table 2: Tensile coupon test results

ID	Specimen	Base Metal Thickness t (in) [mm]	Gauge Length Elongation ΔL_g (%)	Yield Stress[a] $F_{y,0.2}$ (ksi) [MPa]	Yield Stress[b] $F_{y,auto}$ (ksi) [MPa]	Upper Yield Stress $F_{y,upper}$ (ksi) [MPa]	Tensile Strength F_u (ksi) [MPa]	Strain at Tensile Strength ε_u (in/in)	Strain at Rupture ε_r (in/in)
1	362S162-68-W1	0.0717 [1.82]	17.50	61.83 [426.3]	62.19 [428.8]	62.61 [431.6]	79.90 [550.9]	0.1304	>0.17
2	362S162-68-W2	0.0719 [1.83]	17.40	61.02 [420.7]	61.08 [421.1]	61.20 [422.0]	78.34 [540.1]	0.1324	>0.17
3	362S162-68-F1	0.0727 [1.85]	17.78	62.17 [428.6]	61.78 [425.9]	62.84 [433.3]	79.29 [546.7]	0.1230	>0.17
4	362S162-68-F2	0.0713 [1.81]	18.30	58.37 [402.4]	59.09 [407.4]	58.41 [402.7]	77.73 [535.9]	0.1322	>0.17
Mean		0.0719 [1.83]		60.85 [419.5]	61.04 [420.8]	61.26 [422.4]	78.81 [543.4]		
C.o.V		0.0080 [0.21]		0.028 [0.195]	0.023 [0.155]	0.033 [0.229]	0.012 [0.085]		
5	600S137-54-W1	0.0551 [1.40]	21.61	58.35 [402.3]	58.60 [404.0]	58.90 [406.1]	70.27 [484.5]	0.1541	>0.20
6	600S137-54-W2	0.0551 [1.40]	23.51	57.74 [398.1]	57.38 [395.6]	57.87 [399.0]	69.77 [481.0]	0.1772	>0.22
7	600S137-54-F1	0.0546 [1.39]	23.25	56.48 [389.4]	56.69 [390.8]	56.79 [391.5]	69.87 [481.8]	0.1798	>0.22
8	600S137-54-F2	0.0544 [1.38]	23.65	56.48 [389.4]	56.56 [389.9]	56.82 [391.7]	69.72 [480.7]	0.1783	>0.22
Mean		0.0548 [1.39]		57.26 [394.8]	57.31 [395.1]	57.59 [397.1]	69.91 [482.0]		
C.o.V		0.0060 [0.16]		0.016 [0.113]	0.016 [0.112]	0.017 [0.120]	0.004 [0.025]		
9	362T125-68-W	0.0711 [1.81]	18.68	58.91 [406.2]	59.25 [408.5]	59.05 [407.1]	77.91 [537.2]	0.1325	>0.18
10	362T125-68-L	0.0722 [1.83]	18.90	62.54 [431.2]	62.59 [431.5]	62.64 [431.9]	79.40 [547.4]	0.1289	>0.17
11	600T150-54-W	0.0545 [1.38]	21.95	59.55 [410.6]	59.27 [408.6]	59.66 [411.3]	71.31 [491.6]	0.1710	>0.21
12	600T150-54-L	0.0547 [1.39]	23.58	58.80 [405.4]	58.62 [404.2]	58.84 [405.7]	70.67 [487.2]	0.1675	>0.22

[a]The 0.2% offset method is used here

[b]The autographic method used was the averaging of the stress levels at the 0.4% and 0.8% offset intercepts

3. General Test Results

3.1 Unbraced Columns: Experimental Results

The purpose of the single stud tests was to provide a baseline and explore the end condition formed between the studs and tracks. Although not expected to buckle with a globally pinned end condition due to the end bearing and screw connections with the track, global buckling was observed as the primary limit state. Fig. 12 shows the results for all trials of both cross-section types, without sheathing; note that for the loading data for the single stud trials (A1 and B1), a scale factor of 2 was applied to allow for comparison with the other trials that employ doubled studs. With the addition of another stud in the track, but no screw connections between the studs (A2 and B2), an increase in capacity is observed when compared to the scaled single stud capacities. Although the buckling modes were similar, a more rigid end condition is expected as the studs buckled sympathetically and friction may develop between the two studs. With the addition of the fasteners in the web the capacity increased, but was limited by local buckling in the case of the B-series 600S137-54 specimens, as summarized in Table 3.

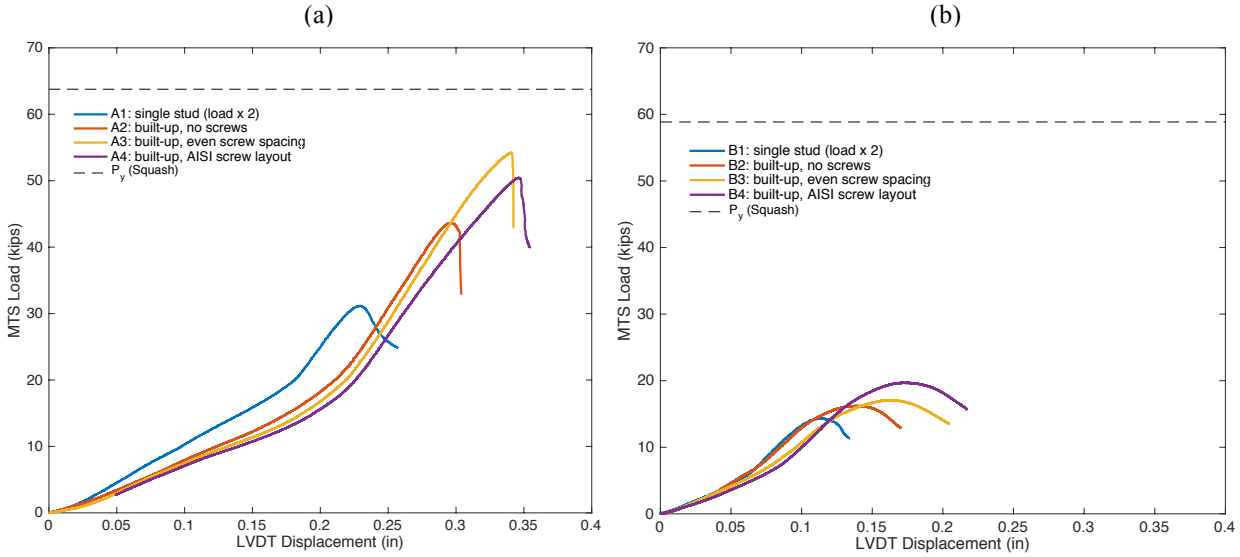

Figure 12: Test data (P-δ) for all unsheathed column trials: (a) 362S162-68 and (b) 600S137-54 specimens

Table 3: Unsheathed specimen experimental results

Trial	Specimen Type	Observed Elastic Buckling Mode	P_u (kips) [kN]	Failure Mode at the Peak Load
A1	Single 362S162-68	FT	15.59 [69.35]	FT
A2	Back-to-Back 362S162-68	FT[a]	43.68 [194.3]	FT[a]
A3	Back-to-Back 362S162-68	D[b]	54.22 [241.2]	L (web, mid-height) [a]
A4	Back-to-Back 362S162-68	D[b]	50.45 [224.4]	L (web, mid-height) [a]
B1	Single 600S137-54	F (minor axis)/FT	7.184 [31.94]	L (lips, mid-height)
B2	Back-to-Back 600S137-54	F (minor axis)[b]	16.22 [72.15]	D/L (lips, mid-height)[a]
B3	Back-to-Back 600S137-54	F (minor axis)[b]	17.08 [75.98]	D/L (lips, mid-height)[a]
B4	Back-to-Back 600S137-54	L (web)[b]	19.70 [87.63]	D/L (lips, mid-height)[b]

[a]non-sympathetic buckling mode (generally symmetric about the minor axis)
[b]sympathetic buckling mode between the two studs (non-symmetric about minor axis)
Note: FT = flexural-torsional, F = flexural, D = distortional, and L = local

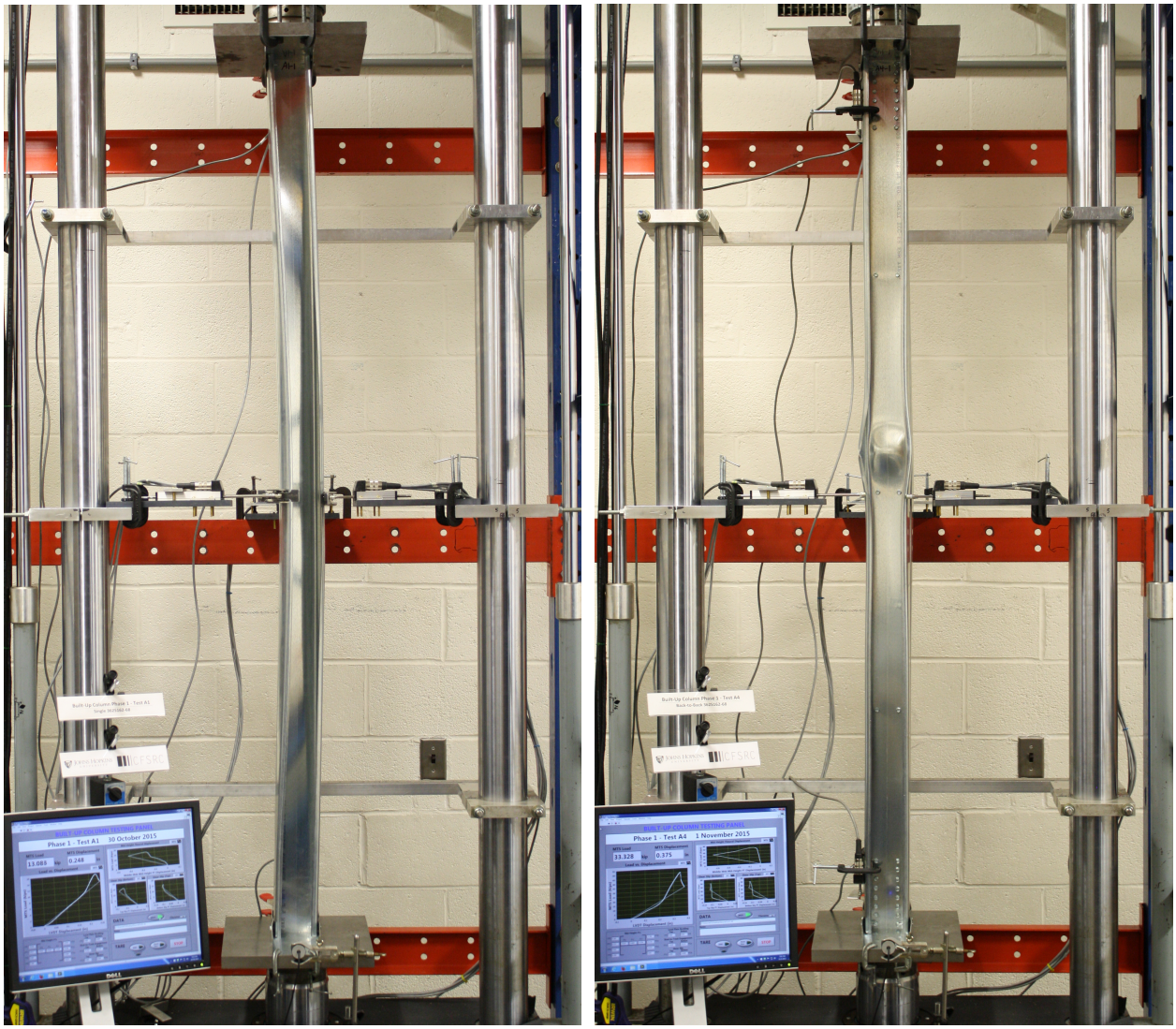

Figure 13: Typical flexural-torsional (left, trial A1) and interacting local/flexural (right, trial A4) buckling failures

Figures 13 and 14 show typical modes of failure reported in Table 3 for the unsheathed columns. Note that the change in initial stiffness in the plots of Fig. 12 are caused by the seating of the column ends in the tracks upon loading. At 6 ft [1.83 m] length, the 362S162-68 stud buckles in a flexural-torsional mode. With the addition of fasteners, the increase in capacity is evident (up to 74% as shown in Fig. 12a) due to the increase in composite action, and the mode shifts from a global to a local mode. Also evident is that the strength of column A4 (with a denser fastener spacing on the web) is less than the strength of column A3; the presence of the end fastener groupings (EFGs) had little to no effect on the buckling deformation and peak capacity, and the observed difference could be attributed to geometric imperfections or stud-to-track end conditions. Vieira (2011) also studied the same 362S162-68 columns at the same length, and results compare reasonably well. In Vieira (2011), the unsheathed 6 ft [1.83 m] column failed in flexural-torsional buckling at a load of 13.59 kips [60.46 kN], a capacity 13% less than the comparable specimen tested in trial A1. Differences in delivered thickness, material yield stress, geometric imperfections, or stud-to-track engagement could account for the discrepancy. The 600S137-54 stud (specimen B1) buckled in a minor-axis flexural mode, as did columns B2 and

B3. Surprisingly, neither stiffness nor strength varied substantially for the back-to-back sections with the addition of the web fasteners. However, an increase in capacity was observed for this stud with the addition of the EFGs, and their presence enforced a sympathetic web local buckling mode. Although the benefit of the EFG is assumed to be to limit end slip and thus maximize composite action in global (flexural) buckling, such a substantial number of fasteners also has an impact on local buckling as observed in this case.

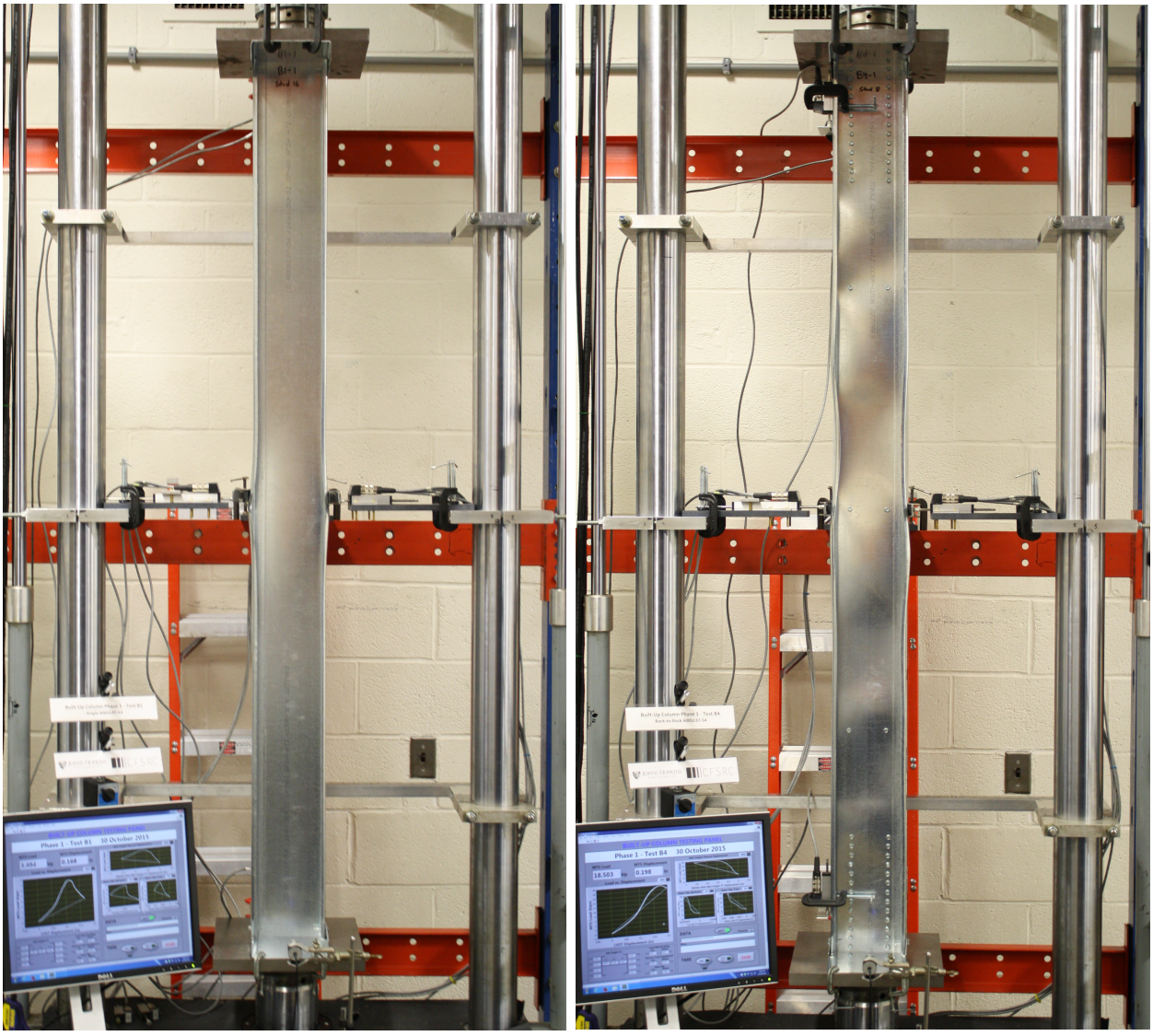

Figure 14: Typical flexural (left, trial B1) and interacting local/flexural (right, trial B4) buckling failures

3.1.1 Southwell Estimation of Column End Conditions

Also sought from the results was an estimate of the end conditions. For trials A1 and B1 with single studs and a single fastener connecting each flange between the stud and track, end conditions closer to the pin-pin case can be expected. However, bearing is also possible and thus it is difficult to know the end condition prior to testing. In the built-up cases (e.g., trials A4 and B4), a shear force couple exists via the stud-to-track screws (see Fig. 6), and in conjunction with the EFGs connecting the webs, a more rigid end condition is expected. The Southwell method

was used to estimate the elastic, minor-axis flexural buckling loads of the columns using position transducer displacement at mid-height, specifically the out-of-plane deflection of the specimens' webs. The critical load is estimated using Eq. 3, with notation similar to Southwell's original form (1932):

$$\delta = P_{cr}\left(\frac{\delta}{P}\right) - \delta_o \tag{3}$$

where δ is the lateral deflection at mid-height, P_{cr} is the estimated elastic minor-axis flexural buckling load (calculated as the slope of the line in a plot of δ/P vs. δ), P is the applied load, and δ_o is any initial deflection in the column, which is ignored when determining the critical load. The method is approximate, but provides some insight.

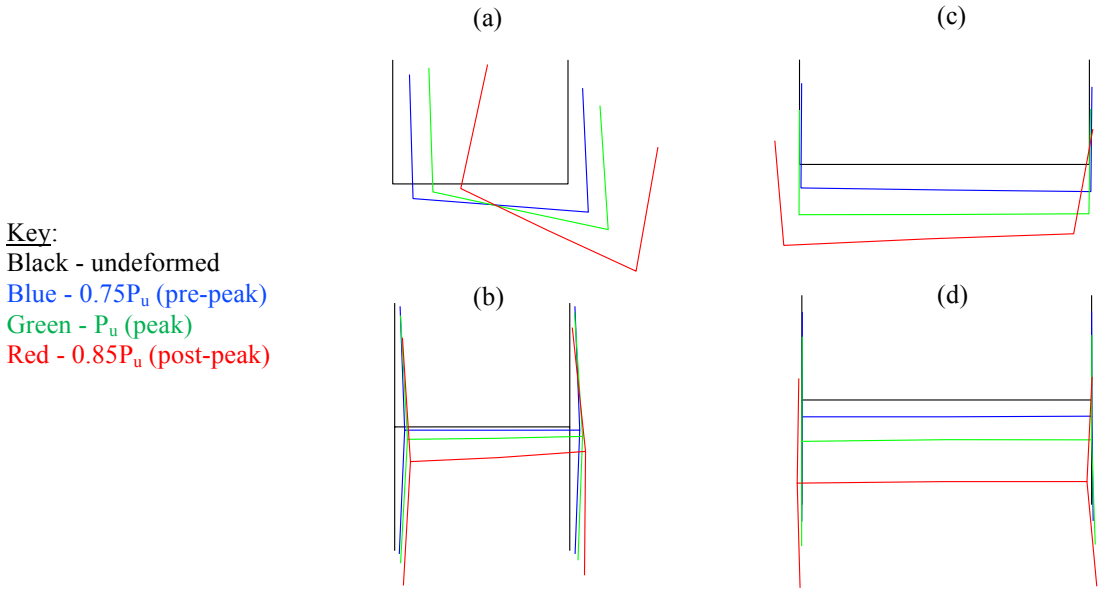

Figure 15: Plots of mid-height cross section displacements/rotations (to scale, from position transducers) for unsheathed trials (a) A1, (b) A4, (c) B1, and (d) B4

Note, that although some columns deformed in a torsional mode at peak load (such as A1), the initial displacements were of flexural type in the linear elastic range of loading. Also, linear P-δ data was extracted from the overall test data for each trial after the point at which the studs' cross sections were recorded to be fully engaged to the tracks by the stud-to-track PTs. Fig. 15 provides the cross-section deformation as recorded by the mid-height PTs at the web (from one end) and the flanges. The different colors represent various stages of loading, with black indicating the base, undeformed state. For each trial, the data before 75% of peak load was reached (the blue cross sections in Fig. 15) was used in the Southwell estimations. Table 4 shows the effective length factors, back-calculated from the Euler formula for critical buckling load, where the critical load is the slope from the Southwell plot. Calculations are performed assuming non-composite action. The presence of local buckling, distortional buckling, torsional buckling, and partially composite action complicate the approximation. Nonetheless, under the stated assumptions, K is between 0.8 and 1.0 for the single studs and 0.5 and 0.6 for the composite studs.

Table 4: Estimation of column end conditions

Specimen	P_{Euler} with K=0.5 (kips) [kN]	P_{Euler} with K=1.0 (kips) [kN]	$P_{cr,Southwell}$ (kips) [kN]	Effective Length Factor, K
A1 (single)	10.45 [46.48]	41.79 [185.9]	10.1 [44.9]	1.00
A4 (built-up)*	20.89 [92.92]	83.57 [371.7]	74.0 [329.]	0.53
B1 (single)	5.897 [26.23]	23.59 [104.9]	9.10 [40.5]	0.81
B4 (built-up)*	11.79 [52.44]	47.18 [209.9]	29.0 [129.]	0.64

*a non-composite calculation is used

3.2 Sheathing-Braced Columns: Experimental Results

Specimens A5-A8 and B5-B8 repeat the previous tests but now with OSB sheathing attached to the flanges of the studs. The results as shown in Fig. 16 and Table 5 are that the impact of the sheathing is more important than the detailing of the all steel back-to-back specimens. Again, the single stud loads are scaled by 2 to compare more directly with the other trials.

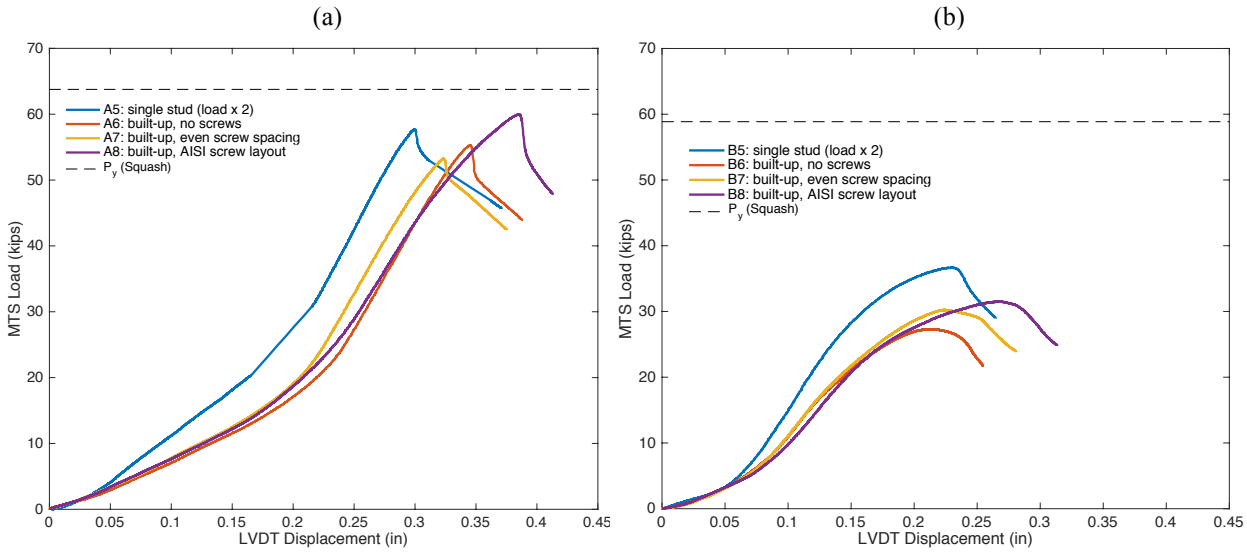

Figure 16: Test data (P-δ) for all sheathed column trials: (a) 362S162-68 and (b) 600S137-54 specimens

Table 5: Unsheathed specimen experimental results

Trial	Specimen Type	Buckling Mode	P_u (kips) [kN]	Failure Mode
A5	Single 362S162-68	L (web, top)	28.87 [128.4]	L (web, top)
A6	Back-to-Back 362S162-68	L (web, top)[a]	55.31 [246.0]	L (web, top)[a]
A7	Back-to-Back 362S162-68	L (web, top)[a]	53.25 [236.9]	L (web, top)[a]
A8	Back-to-Back 362S162-68	L (web, bottom)[b]	59.96 [266.7]	L (web, bottom)[b]
B5	Single 600S137-54	L (web)[a]	18.35 [81.62]	L (web, top)
B6	Back-to-Back 600S137-54	L (web)[a]	27.31 [121.5]	L (web, top)[a]
B7	Back-to-Back 600S137-54	L (web)[a]	30.25 [134.6]	L (web, top)[a]
B8	Back-to-Back 600S137-54	L (web)[a]	31.53 [140.3]	L (web, bottom)[b]

[a]non-sympathetic buckling mode
[b]sympathetic buckling mode
Note: L = local

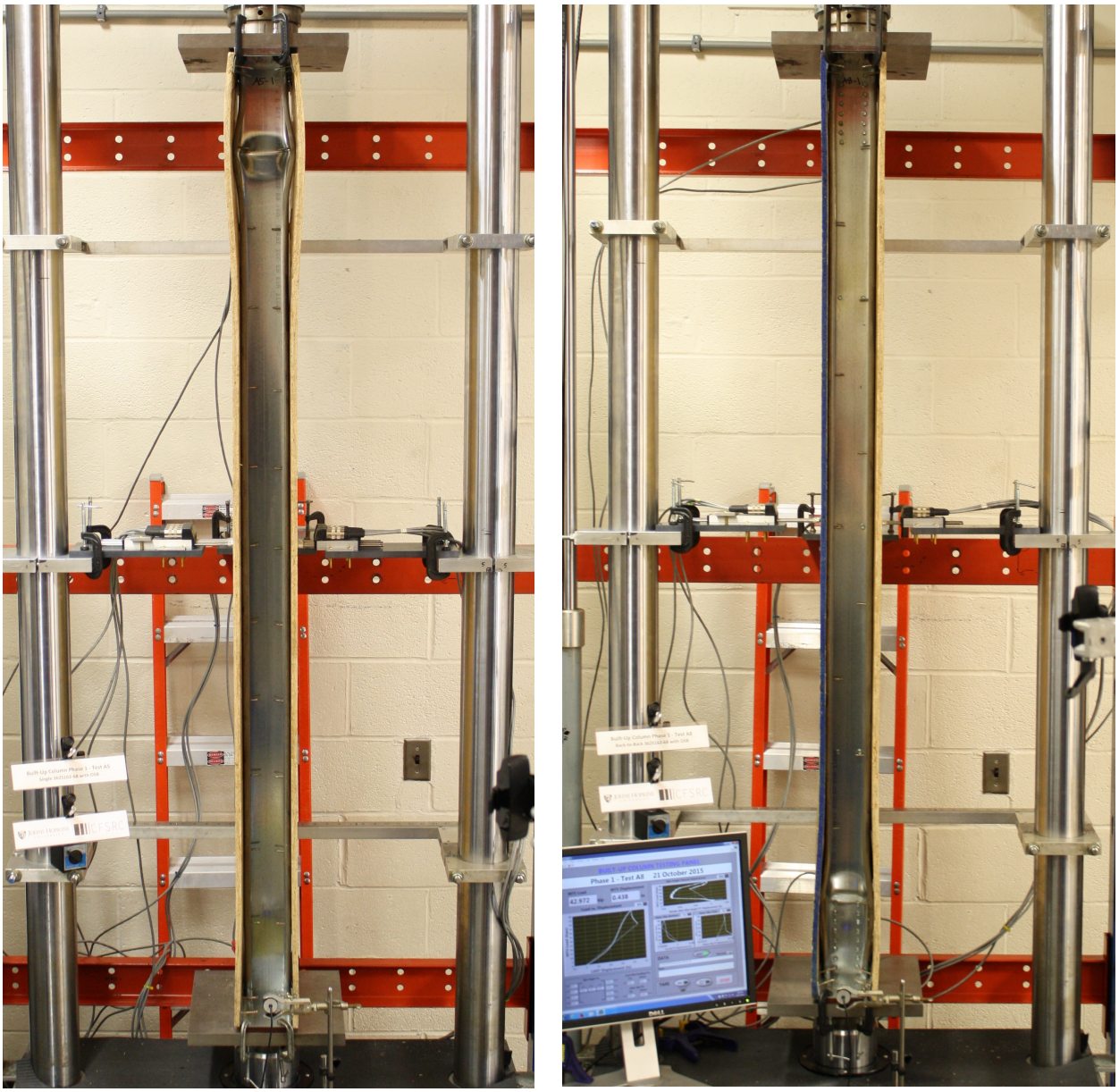

Figure 17: Typical single stud (left, trial A5) and built-up column (right, trial A8) web local buckling failures

Table 5 shows all sheathed trial test results. As shown in Fig. 16, the strength of the screw-fastened columns (A7, A8, B7, and B8) is not significantly larger, since local buckling controlled and the fastener spacings consistently allowed for the local buckling half-wavelengths to develop. The local buckling mode (sympathetic or non-sympathetic) generally yielded the same column strength. Also evident in the plots is the increased stiffness of the single sheathed studs. This is due in part to the 6 in. [15.2 cm] screw longitudinal spacing, which connect the flanges to the OSB on the single studs. The spacing difference between single and back-to-back sheathed columns is shown in Figures 17 and 18; in the back-to-back studs, the spacing is the same, but staggered on one flange at each 6 in. increment. The highest strength of the 362S162-68 sheathed series was recorded in A8 at 59.96 kips [266.7 kN], in which a sympathetic local buckling half-wave developed just above the lower EFG.

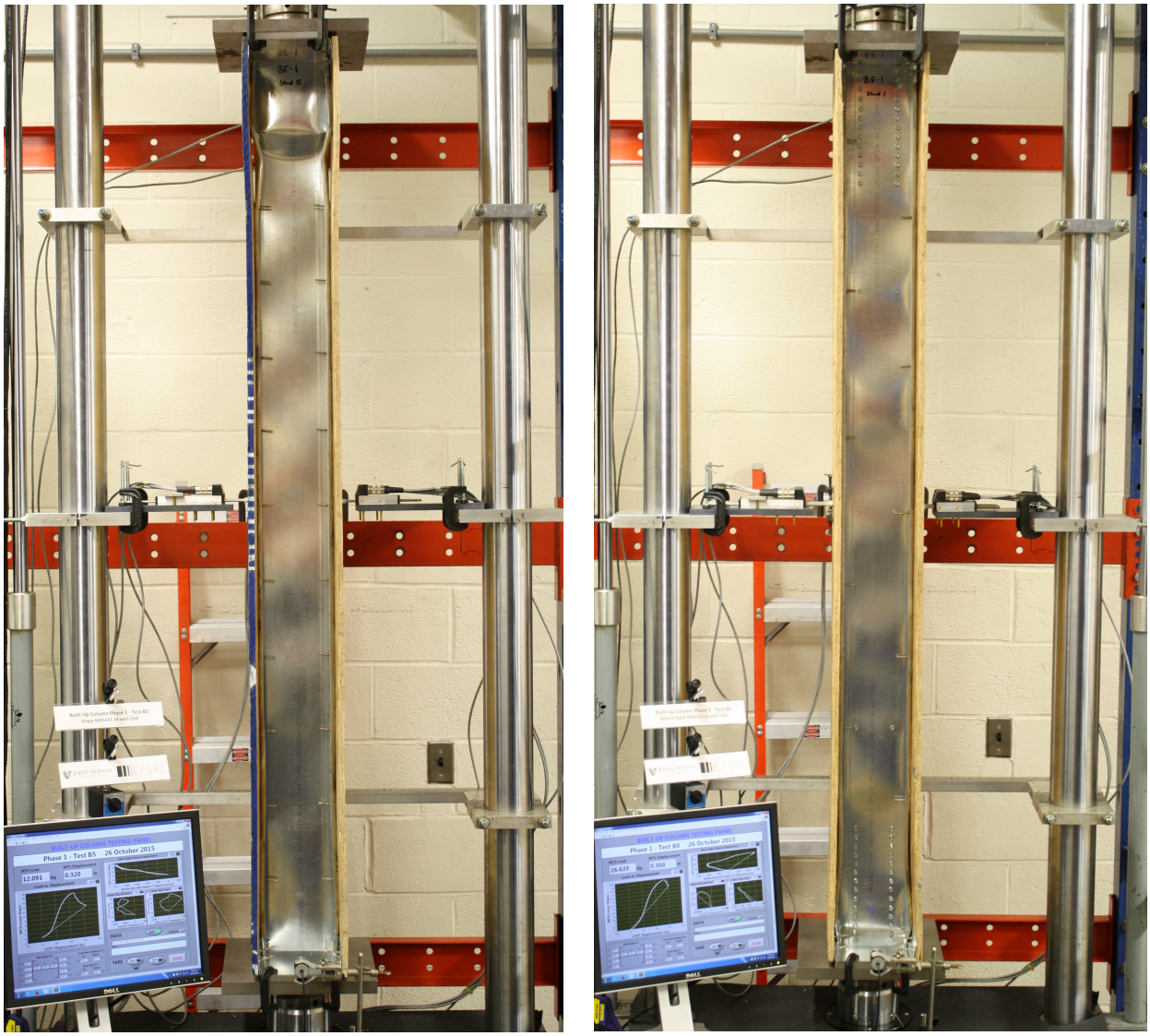

Figure 18: Typical single stud (left, trial B5) and built-up column (right, trial B8) web local buckling failures

Similar buckling and failure modes were observed in the sheathed 600S137-54 series tests (B5-B8). For the built-up specimens B6-B8 the strength increases with the additional detailing. However, the stiffness remains essentially constant across B6-B8. The single stud specimen B5 exhibits the highest stiffness and strength when multiplied by 2 to compare with the back-to-back test results. As in the A5 series the stud-to-sheathing spacing is 6 in., but since there is only one stud it is not staggered as is the case for built-up members and thus the individual flange in the B5 tests has a 6 in. [15.25 cm] stud-to-sheathing fastener spacing. Another test with the staggered layout (as in the built-up columns, with 12 in. [30.5 cm] longitudinal spacing) on this B5 specimen is under way to more fully quantify the single sheathed stud to built-up stud comparison. In trial B8, a sympathetic mode developed, but web crippling at the lower end of the column drove the failure; this may be attributed to a localized moment caused by the differential engagement of each individual stud's web to the track upon initial loading.

3.3 Comparison with DSM predictions

Simple analyses in the finite strip elastic buckling software CUFSM (Schafer and Ádàny 2006) were completed to support a comparison of strength predictions via DSM with test results. The provided comparisons are preliminary. Studs were modeled with nominal dimensions, but yield stresses from coupon tests were applied accordingly. Both pin-pin and fixed-fixed end conditions were modeled in CUFSM, following conventions in Li and Schafer (2010a). OSB boards were modeled using calculated stiffnesses (Table 6): k_x, the lateral translational stiffness; k_y, the out-of-plane translational stiffness; and k_φ, the rotational stiffness as derived and validated by Vieira and Schafer (2013). Fixed, smeared constraints were used to model the web-to-web screws, as shown in Fig. 19. For global buckling analysis all sheathing springs were included in determination of elastic buckling. For distortional buckling analyses only the sheathing rotational spring was included in the elastic buckling model. For local buckling all sheathing springs were ignored. This follows the recommendations of Vieira and Schafer (2013).

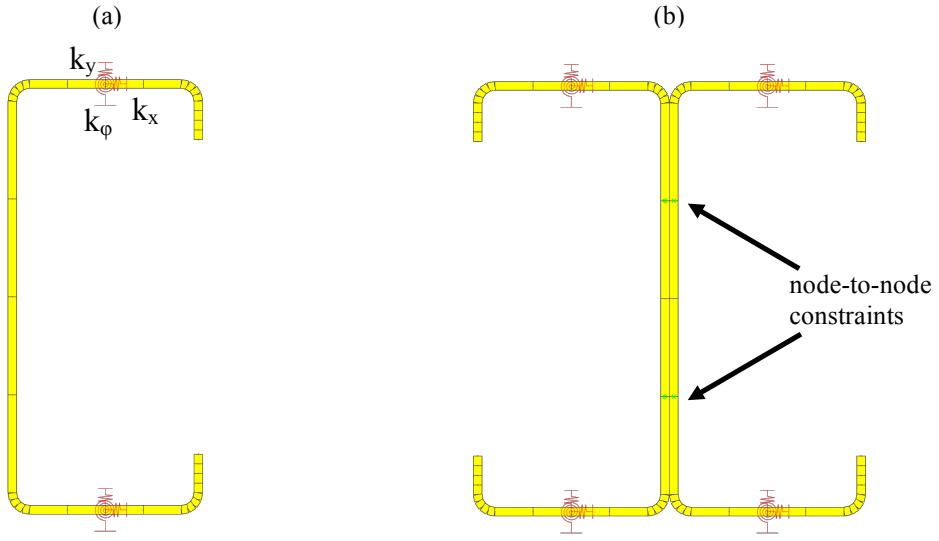

Figure 19: Schematic of smeared spring application in CUFSM for (a) single studs and (b) back-to-back studs

Table 6: Smeared spring stiffnesses used to model sheathing in CUFSM

Stiffness	362S162-68 Trials	600S137-54 Trials	Units
k_x	0.5251	0.3131	(kip/in)/in
k_y*	0.0735	0.1840	(kip/in)/in
k_φ	0.0810	0.0727	(kip × in/rad)/in

*the fully composite k_y was used, see Vieira and Schafer (2013)

Table 7: Comparison of test results with DSM predictions of column strength

Trial	Specimen	P_u (kips) [kN]	Tested Mode	Model End Condition	P_n (kips) [kN]	DSM Mode	P_u/P_n
A1	Single	15.59 [69.35]	FT	pin-pin	8.090 [35.99]	FT	1.93
				fix-fix	20.49 [91.16]	FT	0.76
A2	Built-Up	43.68 [194.3]	FT	fix-fix	40.42 [179.8]	L-G	1.08
A3	Built-Up[a]	54.22 [241.2]	L	fix-fix	52.45 [233.3]	L-G	1.03
A4	Built-Up[b]	50.45 [224.4]	L	fix-fix	52.45 [233.3]	L-G	0.96
A5	Single	28.87 [128.4]	L	pin-pin	26.13 [116.2]	L-G	1.11
				fix-fix	26.69 [118.7]	D	1.08
A6	Built-Up	55.31 [246.0]	L	fix-fix	53.39 [237.5]	D	1.04
A7	Built-Up[a]	53.25 [236.9]	L	fix-fix	53.96 [240.0]	D	0.99
A8	Built-Up[b]	59.96 [266.7]	L	fix-fix	53.96 [240.0]	D	1.11
B1	Single	7.180 [31.94]	L	pin-pin	4.556 [20.27]	L-G	1.58
				fix-fix	10.89 [48.42]	L-G	0.66
B2	Built-Up	16.22 [72.15]	L-D	fix-fix	22.09 [98.24]	L-G	0.73
B3	Built-Up[a]	17.08 [75.98]	L-D	fix-fix	22.91 [101.9]	L-G	0.75
B4	Built-Up[b]	19.70 [87.63]	L-D	fix-fix	22.91 [101.9]	L-G	0.86
B5	Single	18.35 [81.62]	L	pin-pin	14.15 [62.95]	L-G	1.30
				fix-fix	14.30 [63.60]	L-G	1.28
B6	Built-Up	27.31 [121.5]	L	fix-fix	25.49 [113.4]	D	1.07
B7	Built-Up[a]	30.25 [134.6]	L	fix-fix	24.36 [108.4]	D	1.24
B8	Built-Up[b]	31.53 [140.3]	L	fix-fix	24.36 [108.4]	D	1.29

[a]even screw spacings along column length
[b]AISI-based screw spacings (with EFG)

Table 7 shows the results of nominal capacity and prevailing buckling mode from a DSM approach following state-of-the-art design, but still not including discrete springs or other details, compared with the test results. Single studs were modeled with both a pin-pin and fixed-fixed end condition, following the results of the Southwell estimation. Performance of the prediction for the relatively stocky 362S162-68 is good across the specimens with respect to strength prediction less so with respect to limit state prediction. Performance of the prediction for the 600S137-54 overestimates the unsheathed specimens and underestimates the sheathed specimens. Additional consideration needs to be made in more precisely determining the elastic buckling loads, particularly with respect to distortional buckling. This effort is now underway.

4. Discussion

The unsheathed specimens (A1-A4 and B1-B4) specifically illustrate how composite action evolves in built-up cold-formed steel column members. Installed end condition and attachment to secondary members such as track can, along with friction and contact, provide a significant amount of composite action even without explicit inter-connection between built-up members. Connecting the webs of the built-up member regularly, or intensely at the ends, has benefits, but they are less than one might generally expect given the significant amount of composite action realized even without these details.

The presence of sheathing fundamentally alters the nature of composite action in built-up cold-formed steel members. In the studied examples the sheathing, far more than any other detail, establishes the degree of composite action between the members in the built-up section. This suggests that all-steel design for composite action may be inefficient and unnecessary and a more system-level design of cold-formed steel walls should be considered when appropriate.

The sheathing has an effect on both composite action and bracing of the studs. During the tests, outward bending of the track lips was observed, indicating that some axial loads were transferred through the OSB via the track screws, even if the ends of the OSB board were not in contact with the loading platens. Vieira (2011) also observed this behavior. This should be further studied, using different sheathing materials and screw connections to track, and perhaps different instrumentation schemes to quantify the amount of axial load present in the sheathing.

Boundary condition nonlinearity was omnipresent in all of the trials. Whether single, back-to-back, unsheathed, or sheathed, the stud ends engaged the tracks' screws and webs gradually during loading. The change in stiffness is seen in all test data plots, and stud end conditions (how flush the ends are and if the webs or flanges contact the track web first) can drive different failure modes. This behavior is realistic and potentially consistent with installed behavior, but once dead load is present and the stud is fully seated in the track, it may not be relevant to ultimate strength.

Additional analysis is needed on design method predictions for built-up cold-formed steel columns. The elastic buckling approximations made in this paper may be too simple for final use, and deserve further study. This is particularly true for the more locally slender 600S137-54 section. In addition, the modified slenderness ratio for global flexural buckling of AISI-S100-12 needs additional study, as it does not capture the local, distortional, torsional, and flexural-torsional buckling modes. Also, the design calculations should be performed on as-measured instead of nominal dimensions, and this work is already underway.

The observed composite behavior is cross-section and limit state dependent due to the presence of local buckling, distortional buckling, and global torsional modes that are typically ignored in classical considerations of built-up sections. Thus, additional experiments on other cross-sections and member lengths, which are planned, will shed additional light on these issues. In addition, the experiments will be used to develop nonlinear finite element collapse analyses and further expand the parameters with an aim towards developing reliable and robust design methods for built-up cold-formed steel columns.

Testing phases which will immediately follow the tests presented herein will aim to analyze the effect of web screw spacing and layout on distortional and local modes, as well as continue to assess the efficacy of the modified slenderness ratio approach for global buckling with many tests of globally-slender cross-sections of varying dimensions. Future numerical work aims to efficiently model fastener connections in built-up sections for beams and columns in a finite strip modeling framework for calculation of elastic buckling loads and modes for use in determining strength.

5. Conclusions

Built-up columns are frequently used in buildings framed from cold-formed steel and are often found within sheathed walls. Therefore, understanding the behavior and strength of screw-fastened built-up cold-formed steel columns with and without sheathing is important, and design specifications ideally should provide efficient solutions in this common scenario. The tests herein show that without sheathing, an all-steel built-up column is influenced by its end attachment (for example, to a track) nearly as much as interconnections between the built-up

members. Also, friction and end conditions can play an important role in composite action of an all-steel built-up column. With sheathing present, the tests herein show that the sheathing influences composite action and bracing conditions. The restraint of the flanges provided by OSB sheathing engages composite action in the built-up member, largely restricts global buckling modes, partially restricts distortional modes, and modestly changes observed local buckling modes. Preliminary evaluation of potential design methods indicates that care must be taken to correctly approximate the end boundary conditions and the impact of sheathing and inter-connections on the buckling modes. Additional work is needed to provide experimental data on different built-up cross-sections, different fastener details, and different primary limit states. Subsequent tests have been planned and are underway.

Acknowledgements

Research for this paper was conducted with partial U.S. Government support under FA9550-11-C-0028 and awarded by the Department of Defense, Air Force Office of Scientific Research, National Defense Science and Engineering Graduate (NDSEG) Fellowship, 32 CFR 168a. The senior authors would also like to acknowledge support from the Australian Research Council for collaboration on this topic under Discovery Project DP140104464. Special thanks to Nick Logvinovsky for his assistance in lab apparatus assembly, Isaiah Sampson for his assistance in post-processing of laser scan data for geometric imperfection quantification, and Matthew Brandes for his help in preparing coupons for tensile testing. Lastly, thanks to ClarkDietrich Building Systems and Simpson Strong-Tie for graciously providing all CFS sections and screw fasteners, respectively. Any opinions, findings, and conclusions or recommendations expressed in this material are those of the author(s) and do not necessarily reflect the views of the sponsors or other participants.

References

AISC 360 (2010). *Specification for Structural Steel Buildings*, American Institute of Steel Construction, Chicago, IL.

AISI-S100. (2012). *North American Specification for the Design of Cold-Formed Steel Structural Members*, American Iron and Steel Institute, Washington, D.C.

American Society for Testing and Materials (ASTM), Standard Test Methods and Definitions for Mechanical Testing of Steel Products (ASTM370-12a), ASTM, West Conshohocken, PA, 2012.

Anbarasu, M., Kanagarasu, K., Sukumar, S. (2015). "Investigation on the bahaviour and strength of cold-formed steel web stiffened built-up battened columns." *Materials and Structures*, 48(12), 4029-4038.

Dabaon, M., Eloobody, E., Ramzy, K. (2015). "Experimental investigation of built-up cold-formed steel section battened columns." *Thin-Walled Structures*, 92, 137-145.

Dabaon, M., Eloobody, E., Ramzy, K. (2015). "Nonlinear behaviour of built-up cold-formed steel section battened columns." *Journal of Constructional Steel Research*, 110, 16-28.

Fratamico, D.C. and Schafer, B.W. (2014). "Numerical Studies on the Composite Action and Buckling Behavior of Built-Up Cold-Formed Steel Columns." *22nd International Specialty Conference on Cold-Formed Steel Structures*, St. Louis, MO.

Fratamico, D.C., Torabian, S., Schafer, B.W. (2015). "Composite Action in Global Buckling of Built-Up Columns Using Semi-Analytical Fastener Elements." Proceedings of the Annual Stability Conference, Structural Stability Research Council, Nashville, TN.

Georgieva, I., Schueremans, L., Pyl, L. (2012). "Composed columns from cold-formed steel Z-profiles: Experiments and code-based predictions of the overall compression capacity." *Engineering Structures*, 37, 125-134.

Georgieva, I., Schueremans, L., Pyl, L., Vandewalle, L. (2012). "Experimental investigation of built-up double-Z members in bending and compression." *Thin-Walled Structures*, 53, 48-57.

Georgieva, I., Schueremans, L., Pyl, L., Vandewalle, L. (2012). "Numerical study of built-up double-Z members in bending and compression." *Thin-Walled Structures*, 60, 85-97.

Georgieva, I., Schueremans, L., Vandewalle, L., Pyl, L. (2012). "Design of built-up cold-formed steel columns according to the direct strength method." *Procedia Engineering*, 40, 119-124.

Li, Yuanqi, Li, Yinglei, Wang, S., Shen, Z. (2014). "Ultimate load-carrying capacity of cold-formed thin-walled columns with built-up box and I section under axial compression." *Thin-Walled Structures*, 79, 202-217.

Li, Z. and Schafer, B.W. (2010a). "Buckling analysis of cold-formed steel members with general boundary conditions using CUFSM: conventional and constrained finite strip methods." *20th International Specialty Conference on Cold-Formed Steel Structures*, St. Louis, MO.

Liu, J-L., Lue, D., Lin, C. (2009). "Investigation on slenderness ratios of built-up compression members." *Journal of Constructional Steel Research*, 65, 237-248.

Loughlan, J. and Yidris, N. (2014). "The local-overall flexural interaction of fixed-ended plain channel columns and the influence on behaviour of local conditions at the constituent plate ends." *Thin-Walled Structures*, 81, 132-137.

Maia, W.F., Vieira, L.C.M., Schafer, B.W., and Malite, M. (2012). "Numerical and Experimental Investigation of Cold-Formed Steel Double Angle Members Under Compression." *21st International Specialty Conference on Cold-Formed Steel Structures*, St. Louis, MO.

MATLAB 2015b, The MathWorks, Inc., Natick, MA, United States.

Reyes, W. and Guzmán, A. (2011). "Evaluation of the slenderness ratio in built-up cold-formed box sections." *Journal of Constructional Steel Research*, 67, 929-935.

Schafer, B.W. and Ádàny, S. (2006). "Buckling analysis of cold-formed steel members using CUFSM: conventional and constrained finite strip methods." *18th International Specialty Conference on Cold-Formed Steel Structures*, Orlando, FL.

Southwell, R.V. (1932). "On the analysis of experimental observations in problems of elastic stability." *Proceedings of the Royal Society of London A: Mathematical, Physical and Engineering Sciences*. 135 (828), 601-616.

Stone, T.A. and LaBoube, R.A. (2005). "Behavior of cold-formed steel built-up I-sections." *Thin-Walled Structures*, 43(12), 1805-1817.

Torabian, S., Zheng, B., and Schafer, B.W. (2015). "Experimental response of cold-formed steel lipped channel beam-columns" Thin-Walled Structures, 89, 152-168.

Vieira, L.C.M. *Behavior and Design of Sheathed Cold-Formed Steel Stud Walls Under Compression*. Ph.D. Thesis, The Johns Hopkins University; 2011.

Vieira, L.C.M. and Schafer, B.W. (2013). "Behavior and Design of Sheathed Cold-Formed Steel Stud Walls under Compression." *Journal of Structural Engineering*, 139(5), 772-786.

Wang, L. *Structural behaviour of cold-formed steel built-up section beams*. Ph.D. Thesis, The University of Hong Kong; 2015.

Ye, J., Feng, R., Chen, W., and Liu, W. (2016). "Behavior of cold-formed steel wall stud with sheathing subjected to compression." *Journal of Constructional Steel Research*, 116, 79-91.

Young, B. and Chen, J. (2008). "Design of Cold-Formed Steel Built-Up Closed Sections with Intermediate Stiffeners." *Journal of Structural Engineering*, 134, 727-737.

Zhang, J. *Cold-formed steel built-up compression members with longitudinal stiffeners*. Ph.D. Thesis, The University of Hong Kong; 2014.

Zhao, X., Tootkaboni, M., Schafer, B.W. (2015). "Development of a Laser-Based Geometric Imperfection Measurement Platform with Application to Cold-Formed Steel Construction." *Experimental Mechanics*, 55, 1779-1790.